

A Comprehensive Study of Self-Assembled Monolayers of Anthracenethiol on Gold: Solvent Effects, Structure, and Stability

Daniel Käfer,[†] Gregor Witte,^{*,†} Piotr Cyganik,[†] Andreas Terfort,[‡] and Christof Wöll[†]

Contribution from the *Physikalische Chemie I, Ruhr-Universität Bochum, 44780 Bochum, Germany*, and *Institut für Anorganische und Angewandte Chemie, Universität Hamburg, Martin-Luther-King-Platz 6, 20146 Hamburg, Germany*

Received October 27, 2005; E-mail: witte@pc.rub.de

Abstract: The formation and molecular structure of self-assembled monolayers (SAMs) of anthracene-2-thiol (AnT) on Au(111) have been characterized by reflection adsorption infrared spectroscopy, thermal desorption spectroscopy, X-ray photoelectron spectroscopy, near-edge X-ray absorption spectroscopy, scanning tunneling microscopy, and low energy electron diffraction. It is demonstrated that highly ordered monolayer films are formed upon immersion, but their quality depends critically on the choice of solvents and rinsing conditions. The saturated monolayer is characterized by a closed packed arrangement of upright standing molecules forming a $(2\sqrt{3} \times 4)$ *rect* unit cell. At about 450 K a partial desorption takes place and the remaining molecules form a dilute (4×2) -phase with an almost planar adsorption geometry, while further heating above 520 K causes a thermally induced fragmentation. According to their different densities both phases reveal very diverse chemical reactivities. Whereas the saturated monolayer is stable and inert under ambient conditions, the dilute phase does not warrant any protection of the sulfur headgroups which oxidize rapidly in air.

I. Introduction

Self-assembled monolayers (SAMs) have attracted considerable attention because of their versatile possibility of tailoring surface properties such as, e.g., wetting behavior, adhesion, lubrication, and corrosion.¹ In the past the vast majority of related studies have been carried out for thiol-based SAMs with aliphatic backbones such as alkanethiols which can be prepared easily on gold surfaces by immersion.^{2,3} More recently aromatic SAMs have become the focus of interest due to their potential applications in lithography,^{4–6} charge transfer, and electronic functionality.^{7–11} In particular, aromatic SAMs enable fundamental study on issues directly related to molecular electronics,^{12,13} i.e., molecular conductivity,⁹ molecular switching,^{14–18} or molecular transistors.¹⁹

In contrast to alkanethiol-based SAMs, whose structure is found to be largely independent of the chain length, the ordering mechanism and structure of aromatic SAMs is more complex. A striking example of this complexity are SAMs formed from biphenyl derivatives BPh ($\text{CH}_3(\text{C}_6\text{H}_4)_2(\text{CH}_2)_n\text{SH}$). It was shown that changing the parameter n from odd to even leads to pronounced changes in their film structure^{20–23} and to changes in a number of film properties including electrochemical stability,²⁴ stability toward exchange by other thiols,²⁵ and

[†] Ruhr-Universität Bochum.

[‡] Universität Hamburg.

(1) Ulman, A. *Chem. Rev.* **1996**, 96, 1533.

(2) Schreiber, F. *Prog. Surf. Sci.* **2000**, 65, 151.

(3) Love, J. C.; Estroff, L. A.; Kriebel, J. K.; Nuzzo, R. G.; Whitesides, G. M. *Chem. Rev.* **2005**, 105, 1103.

(4) Götzhäuser, A.; Eck, W.; Geyer, W.; Stadler, V.; Weinmann, T.; Hinze, P.; Grunze, M. *Adv. Mater.* **2001**, 13, 806.

(5) Zharnikov, M.; Grunze, M. *J. Vac. Sci. Technol., B* **2002**, 20, 1793.

(6) Felgenhauer, T.; Yan, C.; Geyer, W.; Rong, H. T.; Götzhäuser, A.; Buck, M. *Appl. Phys. Lett.* **2001**, 79, 3323.

(7) Tour, J. M. *Acc. Chem. Res.* **2000**, 33, 791.

(8) Sikes, H. D.; Smalley, J. F.; Dudek, S. P.; Cook, A. R.; Newton, M. D.; Chidsey, C. E. D.; Feldberg, S. W. *Science* **2001**, 291, 1519.

(9) Adams, D. M. et al. *J. Phys. Chem. B* **2003**, 107, 6668.

(10) Smalley, J. F.; Sachs, S. B.; Chidsey, C. E. D.; Dudek, S. P.; Sikes, H. D.; Creager, S. E.; Yu, C. J.; Feldberg, S. W.; Newton, M. D. *J. Am. Chem. Soc.* **2004**, 126, 14620.

(11) Zareie, M. H.; Ma, H.; Reed, B. W.; Jen, A. K. Y.; Sarikaya, M. *Nano Lett.* **2003**, 3, 139.

(12) Flood, A. H.; Stoddart, J. F.; Steuerman, D. W.; Heath, J. R. *Science* **2004**, 306, 2055.

(13) Nitzan, A. *Annu. Rev. Phys. Chem.* **2001**, 52, 681.

(14) Chen, J.; Reed, M. A.; Rawlett, A. M.; Tour, J. M. *Science* **1999**, 286, 1550.

(15) Reed, M. A.; Chen, J.; Rawlett, A. M.; Price, D. W.; Tour, J. M. *Appl. Phys. Lett.* **2001**, 78, 3735.

(16) Li, C.; Zhang, D. H.; Liu, X. L.; Han, S.; Tang, T.; Zhou, C. W.; Fan, W.; Koehne, J.; Han, J.; Meyyappan, M.; Rawlett, A. M.; Price, D. W.; Tour, J. M. *Appl. Phys. Lett.* **2003**, 82, 646.

(17) Donhauser, Z. J.; Mantooth, B. A.; Kelly, K. F.; Bumm, L. A.; Monnell, J. D.; Stapleton, J. J.; Price, D. W.; Rawlett, A. M.; Allara, D. L.; Tour, J. M.; Weiss, P. S. *Science* **2001**, 292, 2303.

(18) Dameron, A. A.; Ciszek, J. W.; Tour, J. M.; Weiss, P. S. *J. Phys. Chem. B* **2004**, 108, 16761.

(19) Kagan, C. R.; Afzali, A.; Martek, R.; Gignac, L. M.; Solomon, P. M.; Schrott, A. G.; Ek, B. *Nano Lett.* **2003**, 3, 119.

(20) Rong, H. T.; Frey, S.; Yang, Y. J.; Zharnikov, M.; Buck, M.; Wühn, M.; Wöll, C.; Helmchen, G. *Langmuir* **2001**, 17, 1582.

(21) Heister, K.; Rong, H. T.; Buck, M.; Zharnikov, M.; Grunze, M.; Johansson, L. S. O. *J. Phys. Chem. B* **2001**, 105, 6888.

(22) Azzam, W.; Cyganik, P.; Witte, G.; Buck, M.; Wöll, C. *Langmuir* **2003**, 19, 8262.

(23) Cyganik, P.; Buck, M.; Azzam, W.; Wöll, C. *J. Phys. Chem. B* **2004**, 108, 4989.

(24) Long, Y. T.; Rong, H. T.; Buck, M.; Grunze, M. *J. Electroanal. Chem.* **2002**, 524, 62.

(25) Felgenhauer, T.; Rong, H. T.; Buck, M. *J. Electroanal. Chem.* **2003**, 550, 309.

electron irradiation²⁶ as well as the possibility to anneal these films at higher temperature yielding ultrahigh quality structures.²⁷

At present the fabrication of electronic devices such as organic field effect transistors (OFETs) has been demonstrated for a variety of organic semiconducting materials.²⁸ A particular promising material is pentacene which reveals one of the largest known charge carrier mobilities among organic materials.²⁹ Previous studies have shown that the performance of such acene-based devices depends critically not only on the ordering of the organic semiconductor films but also on the electronic coupling at the electrodes. In fact, it has been demonstrated that SAM coating of electrodes can enhance the device quality³⁰ which is related to modified electronic surface properties³¹ and/or improved growth of the organic semiconductor films.³² As regards their application as a contact primer, SAMs of high electrical conductivity such as aromatic SAMs are required, whereas aliphatic SAMs are rather good insulators.³³

In view of the successful use of acenes such as pentacene as organic semiconductors, acenethiols form an interesting class of molecules. The band-gap (or HOMO–LUMO separation) decreases with an increasing number of aromatic rings according to the properties of the related acenes, while on the other hand also their solubility decreases significantly. Moreover, synthetic routes become increasingly more difficult which limits the size of available and usable acenethiols. Considering these constraints anthracene-2-thiol (AnT, $C_{14}H_9SH$) is a promising molecule. In fact, previous electrochemical experiments suggest that these molecules reveal even better conductivity than biphenylthiols or terphenylthiols.³⁴ While AnT-films have been studied before by means of XPS and NEXAFS³⁵ detailed information about the microstructure and stability of such films are yet not available. Interestingly, the preparation of ordered AnT-SAMs from DMF-solution has been reported in the latter study, whereas in previous studies on various organothiol-SAMs other solvents such as ethanol typically have been used. In view of the rather promising electronic properties of such conjugated aromatic thiol-SAMs, however, detailed information about the microscopic film structure and an optimized preparation are important prerequisites to study their electronic transport properties and to utilize such films in future devices.

Here we present a comprehensive study of the formation and structure of anthracene-2-thiol SAMs on Au(111). By combining a variety of sensitive techniques including reflection adsorption infrared spectroscopy (RAIRS), thermal desorption spectroscopy (TDS), X-ray photoelectron spectroscopy (XPS), near-edge X-ray absorption spectroscopy (NEXAFS), scanning tunneling microscopy (STM), and low energy electron diffraction (LEED),

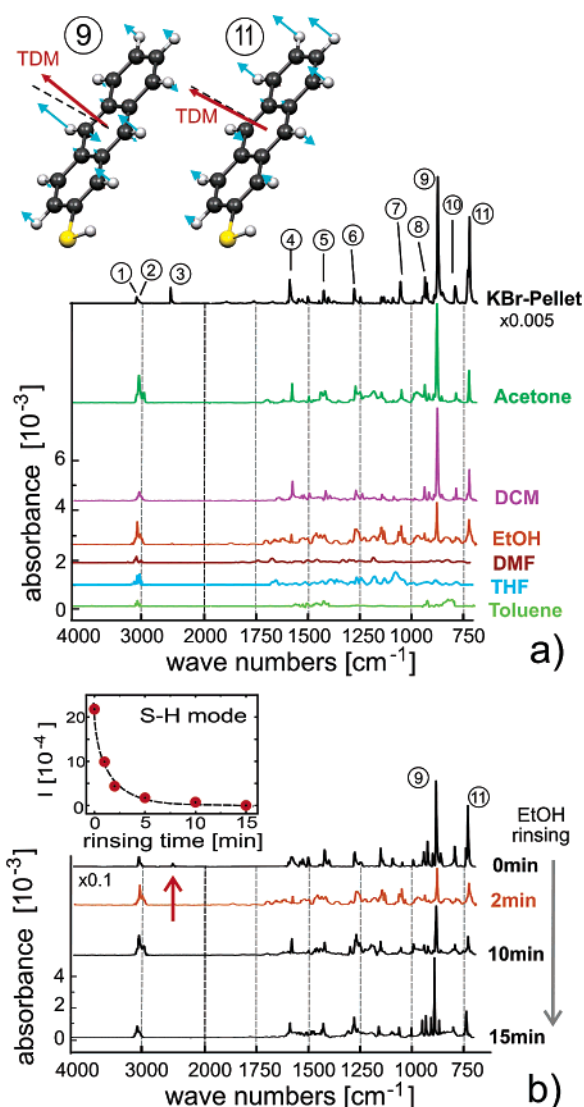


Figure 1. Summary of RAIR spectra recorded for anthracene-2-thiol films prepared by immersion of Au samples (a) from different solvents (rinsing time 2 min) and (b) from ethanolic solution as a function of ethanol rinsing time together with the integrated area of the S–H stretch mode peak (arrow) as a function of the rinsing time (inset). The inset in panel a displays the displacement patterns of the two most intense modes (labeled as 9 and 11).

we were able to precisely characterize the SAM formation and the resulting molecular microstructure. Based on the present measurements we propose an optimized procedure to prepare highly ordered films which is an important prerequisite for their further applications.

II. Results

IR Spectroscopy. To characterize the adsorption properties and the influence of solvents on the resulting film quality, at first IR spectra were recorded for gold samples which were immersed into AnT solutions prepared from different solvents (toluene, THF, DMF, DCM, acetone, and ethanol). In all cases concentrations of 0.1–0.3 mM were used and the samples were immersed for 18–24 h at room temperature and afterward rinsed with the corresponding pure solvents for 2 min. The resulting IR spectra are shown in Figure 1a and are further compared with the corresponding results obtained for a KBr pellet. To assign the vibrational modes and to identify characteristic

- (26) Frey, S.; Rong, H. T.; Heister, K.; Yang, Y. J.; Buck, M.; Zharnikov, M. *Langmuir* **2002**, *18*, 3142.
- (27) Cyganik, P.; Buck, M. *J. Am. Chem. Soc.* **2004**, *126*, 5960.
- (28) Dimitrakopoulos, C. D.; Malenfant, P. R. L. *Adv. Mater.* **2002**, *14*, 99.
- (29) Gundlach, D. J.; Lin, Y. Y.; Jackson, T. N.; Nelson, S. F.; Schlom, D. G. *IEEE Electron Device Lett.* **1997**, *18*, 87.
- (30) Katz, H. E.; Johnson, J.; Lovinger, A. J.; Li, W. J. *J. Am. Chem. Soc.* **2000**, *122*, 7787.
- (31) Alloway, D. M.; Hofmann, M.; Smith, D. L.; Gruhn, N. E.; Graham, A. L.; Colorado, R.; Wysocki, V. H.; Lee, T. R.; Lee, P. A.; Armstrong, N. R. *J. Phys. Chem. B* **2003**, *107*, 11690.
- (32) Hu, W. S.; Tao, Y. T.; Hsu, Y. J.; Wei, D. H.; Wu, Y. S. *Langmuir* **2005**, *21*, 2260.
- (33) Wang, W. Y.; Lee, T.; Reed, M. A. *J. Phys. Chem. B* **2004**, *108*, 18398.
- (34) Scharf, J.; Strehlow, H. H.; Zeysing, B.; Terfort, A. *Solid State Electrochem.* **2001**, *5*, 396.
- (35) Frey, S.; Stadler, V.; Heister, K.; Eck, W.; Zharnikov, M.; Grunze, M.; Zeysing, B.; Terfort, A. *Langmuir* **2001**, *17*, 2408.

Table 1. Calculated Frequencies and Mode Character of the Most Intense Vibrational Modes of Anthracene-2-thiol

| mode | [cm ⁻¹] | mode character |
|------|---------------------|-------------------------|
| 1 | 3047.5 | sym. C–H stretch |
| 2 | 3023.4 | asym. C–H stretch |
| 3 | 2558.6 | S–H stretch |
| 4 | 1616.3 | C–C stretch |
| 5 | 1449.5 | C–C stretch and rocking |
| 6 | 1300.0 | C–H scissoring |
| 7 | 1073.4 | C–H rocking |
| 8 | 953.8 | C–H scissoring |
| 9 | 892.5 | C–H wagging |
| 10 | 806.2 | breathing mode |
| 11 | 735.1 | C–H wagging |

signatures of the various films, the normal modes of AnT have been analyzed on the basis of ab initio calculations. These calculations were carried out for an isolated free AnT molecule including a structure optimization by using the B3LYP algorithm in the Gaussian 98 program package³⁶ with a 6-31+G(d,p) basis set. The calculated frequencies of the most intense modes (*lead bands*) within the recorded energy range are listed in Table 1 together with their mode character.

Surprisingly, the RAIR spectra of films prepared from toluene, THF, or DMF solution reveal a rather weak absorbance and a suppression of numerous vibrational modes as compared to films deposited from other AnT solutions (e.g., acetone or ethanol). Thus the observed mode quenching is not related to orientational effects due to dipole selection rules but instead indicates a fragmentation of the AnT molecules (as confirmed by the TDS results, see below) which hampers the preparation of monolayer films from those solvents. In contrast to that, sharp RAIR spectra with distinct absorption peaks were observed for AnT films prepared from DCM, acetone, or ethanolic solutions.

The molecular orientation in such films can be derived from a detailed analysis of the intensity of vibrational modes with characteristic in-plane or out-of-plane displacement patterns³⁷ and has been carried out previously for phenylene-based aromatic SAMs.^{38,39} We note that, in contrast to high-frequency modes (>2000 cm⁻¹) which are mainly related to diatomic vibrations (such as the C–H stretch mode) in aromatic hydrocarbons,⁴⁰ the lower frequency vibrations of AnT are rather collective modes because of the efficient coupling through the rigid acene backbone. Therefore, the vibrational modes of AnT which are typically observed in the RAIRS spectra have more complex displacement patterns which complicates a quantitative analysis of the molecular orientation. Nevertheless, qualitative information on the molecular ordering can be derived from the intensity of the two dominating absorption lines at 892.5 and 735.1 cm⁻¹ (labeled as mode 9 and 11). Since the corresponding transition dipole moments (TDM) of both modes are nearly perpendicular to the aromatic ring plane [see Figure 1a)], a perfect upright orientation of the aromatic backbone would imply that the corresponding TDMs are parallel to the surface. In that case these vibrations cannot be excited (dipole selection rule) so that such an orientation can be excluded. Moreover,

because a planar adsorption geometry in these films is ruled out on the basis of the STM and LEED data (shown below) the molecules must be tilted. A quantitative analysis of our ab initio calculations yielded angles of the TDM relative to the aromatic plane of 88° and 79° for modes 11 and 9, respectively (see inset in Figure 1a). This results in a larger component of the TDM normal to the surface and thus a larger relative mode intensity for mode 9 which is in close agreement with the experimental observation.⁴¹

Since we have employed X-ray absorption spectroscopy to precisely determine the molecular orientation from the linear dichroism (presented below), the RAIR spectra have not been further analyzed quantitatively. However, a correlation of such RAIR spectra with the outcome of the corresponding structural analysis (presented below) provides a simple empirical signature of the film quality. The intensity ratio of the two dominating absorption lines yields a value of about $I_9/I_{11} \approx 3$ for a saturated monolayer film while it amounts to 1.5 for the pellet.

Interestingly, for films prepared under identical conditions from ethanolic solution, only a ratio of $I_9/I_{11} = 1.7$ was obtained in contrast to preparations from acetone or DCM solution. Because of the common usage of ethanol as solvent for the preparation of organothiol-based SAMs this effect has been studied in more detail. Figure 1b displays a series of corresponding RAIR spectra which were recorded for an unrinsed sample and after different ethanol rinsing times. The RAIR spectrum of the unrinsed sample reveals a very large absorbance which exceeds that of an AnT-SAM prepared from DCM or acetone by more than an order of magnitude and hence reflects the presence of multilayer films. The importance of rinsing is further demonstrated by the evolution of the integrated area of the measured S–H stretch mode peak at 2558.6 cm⁻¹ which is shown in the inset in Figure 1b. While after rinsing of about 5 min this mode is no longer seen, a further reduction of the width and intensity of the vibrational absorption lines in the spectral region of 900–1400 cm⁻¹ was still obtained upon additional rinsing. This is attributed to a slow removal of thin multilayer films by ethanol where AnT molecules presumably adopt a random orientation.

This is again evidenced by the intensity ratio of the two most intense modes. While their ratio amounts to 1.5 for the unrinsed sample which equals the value obtained for the pellet, it yields 1.7 after 2 min of rinsing and increases to 2.6 after 10 min before it reaches finally a value of 3.0 after 15 min of rinsing with pure ethanol. This result emphasizes the importance of proper rinsing to ensure the formation of well-defined monolayer films and to avoid precipitation of multilayer films upon immersion.

Although characteristic intensity ratios were observed in the RAIR spectra of AnT-monolayer films prepared from acetone or DCM solutions, no LEED patterns could be observed for these films in contrast to films prepared from ethanolic solution (see below). This demonstrates that RAIRS provides valuable information about the average molecular orientation but not on the lateral molecular structure. Therefore we have focused on ethanolic preparation to determine also the molecular structure within the AnT-monolayer films.

(36) Gaussian 98, revision A.11.1; Gaussian, Inc.: Pittsburgh, PA, 2001.

(37) Parikh, A. N.; Allara, D. L. *J. Chem. Phys.* **1992**, *96*, 927.

(38) Arnold, R.; Terfort, A.; Wöll, Ch. *Langmuir* **2001**, *17*, 4980.

(39) Azzam, W.; Wehner, B. I.; Fischer, R. A.; Terfort, A.; Wöll, Ch. *Langmuir* **2002**, *18*, 7766.

(40) Huneycutt, A. J.; Casasa, R. N.; McCall, B. J.; Chung, C. Y.; Lee, Y. P.; Saykally, R. J. *ChemPhysChem* **2004**, *5*, 321.

(41) To simulate the effect of adsorption on these two modes, their frequencies and TDM have also been calculated for an AnT molecule bound covalently through the sulfur to a gold atom. This yielded frequency shifts of 7.6–7.8 cm⁻¹ and a homogeneous shift of the TDM angles relative to the aromatic backbone of 4°–5° for both modes.

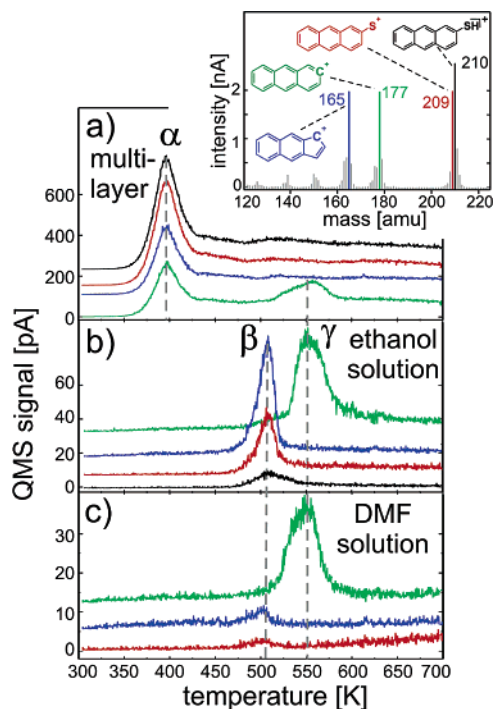


Figure 2. Series of thermal desorption spectra (a) for multilayer films of anthracene-2-thiol on Au(111) and monolayer films prepared from (b) ethanolic solution and (c) DMF solution recorded for a heating rate of $\beta = 3$ K/s. The inset shows the mass spectrum of the AnT gas phase together with the characteristic fragments.

Thermal desorption spectroscopy was used to characterize the various preparation conditions and the thermal stability of the AnT films. To afford a characterization of fragments formed upon ionization in the mass spectrometer at first a gas-phase mass spectrum was recorded for AnT vapor produced by evaporation of solid AnT from a crucible in front of the QMS. The inset of Figure 2a shows a typical mass spectrum which reveals the most probable fragments at $m/z = 209$, 177 , and 165 amu besides the signal of the molecule ion ($m/z = 210$ amu).

Next, thermal desorption spectra were measured for AnT films prepared by various rinsing conditions. Figure 2a displays a TD spectrum recorded after immersion of a gold sample in ethanolic solution without further rinsing before drying. The main signature is a pronounced desorption peak (labeled as α) starting at about 360 K with a maximum around 395 K which was observed for the mass of the molecule ion as well as for all recorded fragments. Since the peak intensity, which is related to the coverage, is about an order of magnitude larger than the corresponding signals recorded for a well-defined monolayer, it has been attributed to multilayer desorption. This assignment is corroborated by our temperature-dependent XPS data presented below. A further analysis (see, e.g., ref 42) shows that the desorption peak α is well described by a kinetics of order zero which yields an intensity of the ascending flank of the desorption peak according to $\ln I \propto -\Delta E_{\text{des}}/RT$. From the slope of the linear curve, an activation energy for desorption of $\Delta E_{\text{des}} = 122 \pm 20$ kJ/mol was derived. This value compares reasonably with the standard sublimation enthalpy of anthracene $H_{\text{sub}} = 100$ kJ/mol⁴³ when considering a somewhat larger

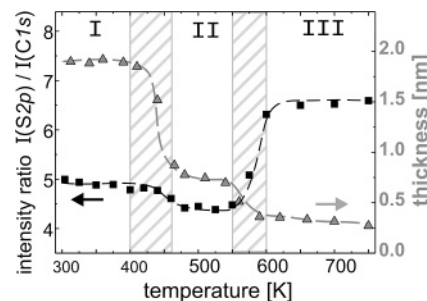


Figure 3. Evolution of the ratio of the S2p and C1s photoelectron intensities and the effective film thickness of an unrinsed anthracene-2-thiol film as a function of the annealing temperature.

polarizability of AnT compared to anthracene. At higher temperatures a further desorption peak was observed at about 550 K for the fragment with $m/z = 177$ amu, while other desorption peaks could not be resolved because of the rather high background signal from multilayer desorption.

Much better resolved TD spectra with a low background signal were obtained for AnT films which had been thoroughly rinsed as shown in Figure 2b for a preparation from ethanolic solution. In that case only two distinct desorption peaks (denoted as β and γ) were observed at 505 and 550 K, respectively. While the β peak could be recorded for different fragment masses, the γ peak appears only at the mass of the sulfur free fragment ($m/z = 177$ amu) and hence indicates a dissociative desorption in the latter case. Note that the small signal at the mass $m/z = 210$ amu in Figure 2b is not related to molecule ions but is caused by ^{13}C containing isotopomers of the $\text{C}_{14}\text{H}_9\text{S}^+$ ion. Using the Redhead formula⁴⁴ with a typical preexponential factor of 10^{13} s^{-1} activation energies for desorption of 132 and 144 kJ/mol, respectively, were calculated from the temperature of the desorption maximum for both desorption peaks.

For comparison additional TD spectra were also recorded for AnT films prepared from DMF solution because such a preparation has been reported in a previous study.³⁵ In contrast to the ethanolic preparation, however, almost no β -peak and only a γ -peak were observed in the corresponding TD spectra for the DMF preparation (see Figure 2c). The absence of any desorption signals related to $\text{C}_{14}\text{H}_9\text{S}^+$ ions as well as the distinctly reduced intensity of the γ -peak indicate a rather poor quality of AnT films with low density upon DMF preparation which is in line with the conclusions drawn from the RAIRS measurements.

XPS. To characterize the thermal and chemical stability of AnT films, temperature-dependent XPS measurements were carried out using Al K_{α} radiation. Figure 3 displays the intensity ratio of the S2p and C1s photoelectron peaks measured for an AnT film prepared from ethanolic solution without rinsing as a function of the annealing temperature together with the resulting effective film thickness (grey data points). The corresponding XP spectra were recorded during cooling after the sample was held at the elevated temperature for 1 min and the energy scale of all spectra was referenced to the $\text{Au}4f_{7/2}$ peak at a binding energy of 84.0 eV. The film thickness was determined from the corresponding ratio of the C1s and $\text{Au}4f$ intensities which was calibrated by additional measurements for an octadecane-

(42) Hänel, K.; Söhnchen, S.; Lukas, S.; Beernink, G.; Birkner, A.; Strunskus, T.; Witte, G.; Wöll, Ch. *J. Mater. Res.* **2004**, *19*, 2049.

(43) Oja, V.; E. M. Suuberg, E. M. *J. Chem. Eng. Data* **1998**, *43*, 486.

(44) Redhead, P. A. *Vacuum* **1962**, *12*, 203.

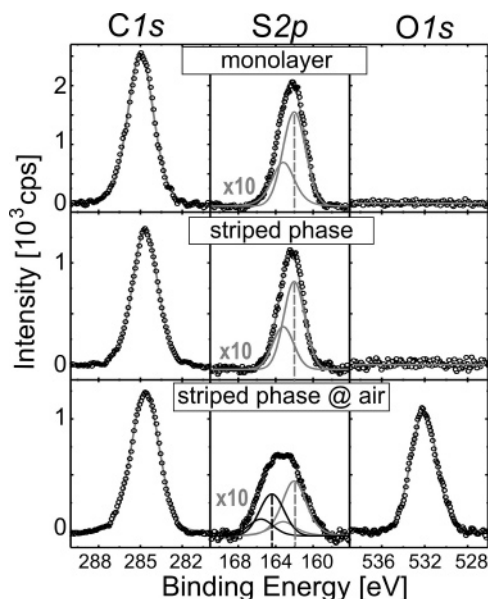


Figure 4. Summary of XP spectra after a linear background subtraction of the C1s, S2p, and O1s regions for an anthracene-2-thiol monolayer and after heating to 500 K. The spectra in the last row were recorded after exposure of the heated films to air.

thiol SAM on Au(111) used as a reference with an effective height of 1.75 nm. The data show a stepwise character which allows an identification of three different regimes (labeled as I–III). Above 400 K a significant reduction of the film thickness takes place due to multilayer desorption. The weak reduction of the intensity ratio of the S2p and C1s lines can be attributed to the orientational ordering of the thiolate monolayer (regime II) which is attached to the substrate through the sulfur headgroup and thus causes a small attenuation of the photoelectrons through the backbone.⁴⁶

Above about 550 K a further decrease of the film thickness takes place which is accompanied by a significant increase of the S/C intensity ratio. Together with the appearance of the γ -desorption peak only for a sulfur-free fragment at that temperature, this indicates a thermally induced fragmentation and desorption of the aromatic backbone of AnT leaving sulfur species at the surface.

For a more precise analysis of the stoichiometry and stability of AnT-SAMs additional XPS data were recorded for monolayer films prepared from ethanolic solution by carefully rinsing (see Figure 4). Since no further decrease of the C1s line intensity was found upon annealing to 450 K they were considered as saturated monolayers. A quantitative analysis of the C1s and S2p_{3/2} line intensities, determined by integration of the fitted Gaussians after a linear background subtraction and in consideration of the corresponding photoelectron cross sections (Scofield factors), yielded a stoichiometric ratio of 13.9 ± 0.4 for such monolayers. This value is in excellent agreement with the C/S ratio of 14:1 in anthracene-2-thiol. No O1s signal was

observed which reflects a rather good shielding of the sulfur headgroups from oxygen through a close-packed monolayer film.

To characterize the diluted film phase formed upon partial desorption of AnT related to the β -peak in the TDS data, further XPS data were recorded after heating a saturated monolayer at 500 K for 5–10 min. A quantitative analysis of the carbon signal shows that the coverage of the heated film, which is denoted as the *striped phase* according to the structural characterization presented later, is reduced to 52% of the saturated monolayer.

In addition, the chemical stability of the striped phase especially against oxidation was characterized by recording XPS data after this phase had been exposed to air for about 5 min. As displayed in Figure 4 this exposure leads to a significant oxygen signal and a distinct broadening of the S2p doublet which is well described by the appearance of a second sulfur species with a S2p_{3/2} binding energy of 164.3 eV. This shift of 2.3 eV toward higher binding energies indicates a (partial) oxidation of the sulfur headgroup and thus demonstrates that the diluted striped phase does not provide any protection against oxidation of the sulfur group, in contrast to the close-packed film (see above).

Interestingly, after reimmersion of such partially oxidized films into ethanolic solution, no oxygen was observed in the corresponding XPS data which indicates a substantial weakening of the sulfur–gold interaction upon oxidation of the sulfur headgroups.

NEXAFS. To characterize the orientational order in the AnT films, X-ray absorption spectroscopy measurements were carried out for AnT films prepared using different procedures which are summarized in Figure 5. To provide a reference system, at first NEXAFS spectra were recorded for AnT multilayers prepared from ethanolic solution without further rinsing. As shown in Figure 5a a common signature in the corresponding spectra includes distinct resonances at around 285 eV which are assigned to excitations of the C1s electrons into closely spaced unoccupied π^* -orbitals. The broad resonance around 293.5 eV is attributed to excitations into σ^* -orbitals.^{47,48} To clarify the fine structure of the π^* -resonances an enlarged view of this spectral region (283.5 to 290 eV) is displayed in the insets in Figure 5. Clearly, the presence of at least three distinct components at 284.52, 285.05, and 285.88 eV (labeled by 1, 2, and 3 in the inset in Figure 5a) can be identified. Similar fine structures with closely spaced π^* -resonances have been observed before in NEXAFS experiments also for other adlayers of aromatic molecules such as pentacene, perylene, or naphthalene.^{42,49,50} This splitting into subresonances results from initial state effects due to slight differences in the chemical coordination of the carbon atoms within the aromatic molecule as well as from final state effects (caused by different positions of the core hole within the molecule).^{48,50}

The theoretical analysis shows that the intensity of the π^* resonances depends on the relative orientation of the electrical field vector \mathbf{E} of the incident synchrotron light and is given by $I_{\pi^*} \propto |\mathbf{E} \cdot \mathbf{T}|^2$, where \mathbf{T} denotes the transition dipole moment

(45) The mean free paths were calculated by using the Gries formula in the program *electron inelastic-mean-free-path v.1.1* provided by the National Institute of Standards and Technology, NIST (USA).

(46) Inelastic mean free paths of the S2p and C1s photoelectron values of $\lambda(\text{S2p}) = 37 \text{ \AA}$ and $\lambda(\text{C1s}) = 34 \text{ \AA}$, respectively, have been calculated for anthracene.⁴⁵ Since these values are much larger than the effective film thickness of the unrinsed samples and monolayers, the self-attenuation has not been further considered.

(47) Yokoyama, T.; Seki, K.; Morisada, I.; Edamatsu, K.; Ohta, T. *Physica Scripta* **1990**, 41, 189.

(48) Agren, H.; Vahtras, O.; Carravetta, V. *Chem. Phys.* **1995**, 196, 47.

(49) Söhnchen, S.; Lukas, S.; Witte, G. *J. Chem. Phys.* **2004**, 121, 525.

(50) Hollauer, E.; Prucolo, E.; Rocco, M. L. M.; Netto, A. D. P.; Schöll, A.; Fink, R. *J. Braz. Chem. Soc.* **2005**, 16, 31.

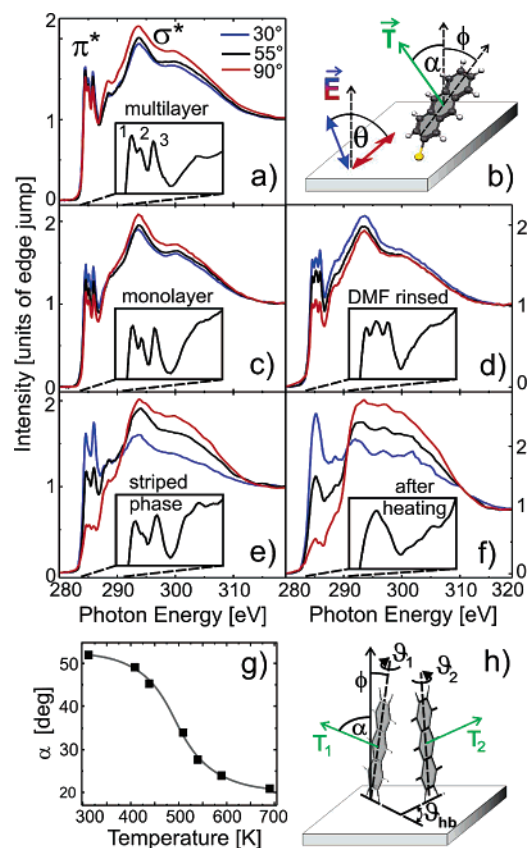


Figure 5. Series of NEXAFS spectra of AnT films prepared from different solutions and after various annealing treatments recorded for different angles of incidence of the synchrotron light according to the experimental geometry shown in panel b. The insets in all spectra display a magnification of the π^* -region (283.5–290 eV) recorded at an angle of 55°. The evolution of the molecular orientation as a function of the annealing temperature is shown in panel g. The relative orientation of the transition dipole moments in aromatic films with a herringbone arrangement together with the definition of characteristic angles describing the molecular orientation is depicted in panel h.

which is oriented normal to the ring plane of the aromatic molecules.⁵¹ For a substrate of 3-fold symmetry and linear polarized light with a degree of polarization, P , this expression can be written as

$$I_{\pi^*} \propto P \cos^2 \theta \left(\frac{3 \cos^2 \alpha}{2} - \frac{1}{2} \right) + \frac{\sin^2 \alpha}{2}$$

where α and θ denote the angles between \mathbf{T} and the surface normal and between \mathbf{E} and the surface normal, respectively, as depicted in Figure 5b. Thus, from NEXAFS measurements carried out for different angles of incidence of the incoming synchrotron light, the average tilt angle of \mathbf{T} relative to the sample normal, α , can be determined quantitatively. If the aromatic molecular plane is tilted by ϕ relative to the sample normal and further twisted along the (long) molecular axis by ϑ the orientation of \mathbf{T} relative to the sample normal can be expressed by $\cos \alpha = \sin \phi \cos \vartheta$.²⁰ Sometimes the quantitative analysis of NEXAFS data is complicated by the presence of differently oriented molecules in a unit cell. In the case of a herringbone-type packing as depicted in Figure 5h, both molecules adopt the same tilt angle ϕ but reveal different twist

angles of their aromatic planes, ϑ_1 and ϑ_2 . In the case of a symmetric arrangement these twist angles can be related to the herringbone angle by $\vartheta_{1,2} = \pm \vartheta_{\text{hb}}/2$. Since the π^* resonance intensities of the two molecules $I_{\pi^*}(T_1)$ and $I_{\pi^*}(T_2)$ add up incoherently, the azimuthal averaging can be carried out separately for each molecule within the unit cell and hence yields the total intensity

$$I_{\pi^*} = \frac{1}{2} [I_{\pi^*}(T_1) + I_{\pi^*}(T_2)] \\ \propto \frac{1}{2} P \cos^2 \theta \left(3 \sin^2 \phi \cos^2 \frac{\vartheta_{\text{hb}}}{2} - 1 \right) \\ + \frac{1}{2} \sin^2 \alpha \arccos \left(\sin \phi \cos \frac{\vartheta_{\text{hb}}}{2} \right)$$

For the multilayer film no distinct intensity variation of the π^* resonances was found in the NEXAFS spectra recorded at different angles of incidence which indicates the presence of orientational disorder.⁶² NEXAFS spectra obtained for the saturated AnT monolayer reveal a small but distinct dichroism (Figure 5c). Assuming that the herringbone packing angle in AnT films is similar to that in anthracene bulk crystals ($\vartheta_{\text{hb}} = 50^\circ$ ⁵²) the quantitative analysis yields an average tilt angle of $\phi = 43^\circ$.

An even more pronounced dichroism was observed for the striped phase obtained after heating the saturated monolayer to 500 K. In that case the analysis described above yields an average tilt angle of the transition dipole moment of $\alpha = 23^\circ$. This orientation suggests a rather flat adsorption geometry which is also evidenced by the electron diffraction measurements discussed below. In this phase the adsorption is mainly stabilized by the interaction of the AnT ring plane with the substrate which excludes a side-on-edge herringbone packing motif. Therefore the tilt angle of the molecular plane is simply related to the orientation of the transition dipole moment and yields a value of $\phi = 90^\circ - \alpha = 67^\circ$. Moreover, for this phase the corresponding π^* resonances are significantly broadened as compared to the saturated monolayer. For the well resolved π_3^* subresonance, a fwhm of 0.7 eV was obtained for the saturated monolayer (Figure 5c), while a value of 0.95 eV was derived for the striped phase (Figure 5e). A similar broadening has been observed before upon adsorption of various aromatic molecules on metal surfaces, e.g., for pentacene on Au(111).⁵³ In that case the molecules adsorb with their ring plane parallel to the metal surface to maximize the chemical coupling of the aromatic

(51) Stöhr, J. *NEXAFS Spectroscopy*; Springer, New York, 1992; Vol. 25.

- (52) Pratt, C.; Brock, J. D.; Dunitz, W. *Acta Crystallogr., Sect. B* **1990**, *46*, 795.
 (53) Beermann, G.; Strunskus, T.; Witte, G.; Wöll, Ch. *Appl. Phys. Lett.* **2004**, *85*, 398.
 (54) Edinger, K.; Götzhäuser, A.; Demota, K.; Wöll, C.; Grunze, M. *Langmuir* **1993**, *9*, 4.
 (55) Poirier, G. E. *Langmuir* **1997**, *13*, 2019.
 (56) Dhirani, A. A.; Zehner, R. W.; Hsung, R. P.; Guyot-Sionnest, P.; Sita, L. R. *J. Am. Chem. Soc.* **1996**, *118*, 3319.
 (57) Jin, Q.; Rodríguez, J. A.; Li, C. Z.; Darici, Y.; Tao, N. J. *Surf. Sci.* **1999**, *425*, 101.
 (58) Azzam, W.; Fuxen, C.; Birkner, A.; Rong, H. T.; Buck, M.; Wöll, C. *Langmuir* **2003**, *19*, 4958.
 (59) Yang, G. H.; Liu, G. Y. *J. Phys. Chem. B* **2003**, *107*, 8746.
 (60) Dishner, M. H.; Hemminger, J. C.; Feher, F. J. *Langmuir* **1997**, *13*, 2318.
 (61) Shaporenko, A.; Cyganik, P.; Buck, M.; Terfort, A.; Zharnikov, M. *J. Phys. Chem. B* **2005**, *109*, 13630.
 (62) Note that the absence of any dichroism would also be expected if the average tilt angle of the transition dipole moment relative to the sample normal α of all molecules equals the magic angle⁵¹ which amounts to 53° for the presently used degree of polarization.

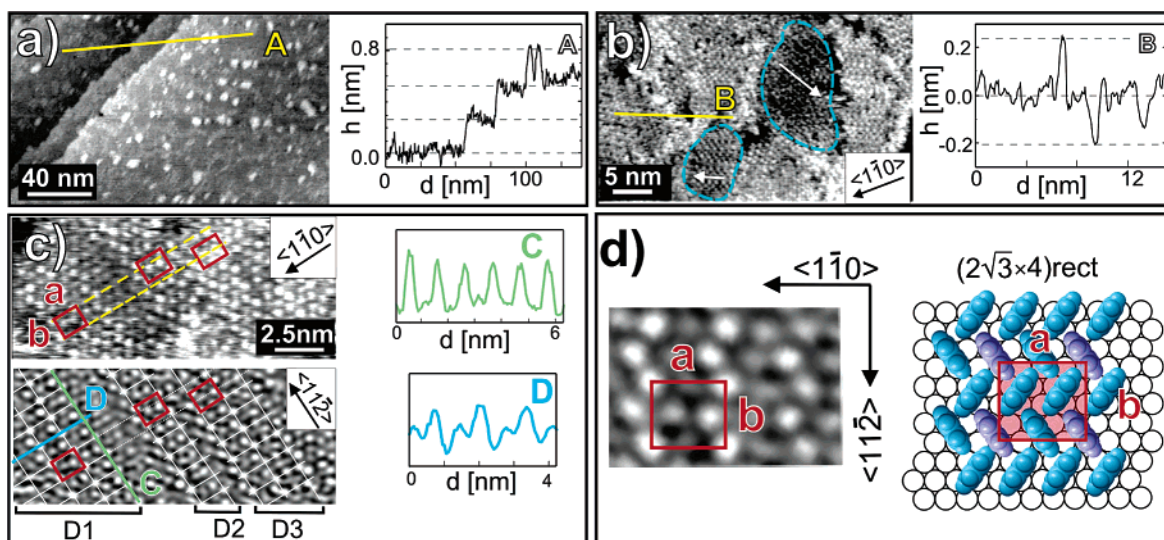


Figure 6. Summary of STM data obtained for a saturated AnT monolayer on Au(111) prepared from ethanolic solution. Panels a and b display large scale STM micrographs together with corresponding line scans showing the presence of substrate islands and rotational domains. In panel c, a high-resolution STM image (before and after FFT filtration) is presented together with the corresponding line scans which allows identification of the molecular unit cell (marked in red) and reveals the presence of three different translational domains denoted by D1, D2, and D3. All images were recorded at $U = -200$ mV and $I = 200$ pA. Panel d displays a magnification of the high-resolution image with the superimposed unit cell and a hard sphere structure model of the corresponding $(2\sqrt{3} \times 4)$ rect phase.

system with the substrate.⁵¹ Further heating above 550–600 K results in a significant reduction of the C1s NEXAFS raw data and a loss of the distinct π^* resonances. Instead only a rather broad π^* resonance remained which indicates a fragmentation of the aromatic backbone.

For the sake of completeness, also NEXAFS data for AnT films prepared from DMF solutions have been recorded. The corresponding spectra reveal a slightly different signature of the π^* -resonances together with a larger dichroism as compared with the saturated monolayer (see Figure 5d). A quantitative analysis yielded an average tilt angle of $\phi = 52^\circ$.

Evidently, the transition from a saturated monolayer toward the striped phase upon heating is accompanied by a molecular reorientation. To monitor the temperature dependence of this reorientation in more detail a series of NEXAFS spectra was recorded as a function of the annealing treatment. Starting from a saturated monolayer, the films were successively heated for about 1 min at the given temperature and the corresponding spectra were recorded during cooling. Figure 5g summarizes the resulting orientation of the dipole moment α which reveals a continuous molecular reorientation from an upright orientation at 300 K toward nearly flat-lying molecules at elevated temperature. Most likely, such a transition of the molecular orientation proceeds via domains of different structures which change their relative size with increasing temperature and hence give rise to a continuous variation of the measured average molecular orientation.

STM. The STM data which were recorded for a saturated AnT monolayer on Au(111) prepared from ethanolic solution are summarized in Figure 6. Data acquired at larger scale are presented in Figure 6a) and their comparison with the analogous images of clean Au substrates (not shown here) reveals that the formation of the AnT films is accompanied by an appearance of small islands having diameters of about 5–10 nm. These islands reveal a characteristic height of about 0.26 nm (see Figure 6a) which is in close agreement with the interlayer

spacing of (111) planes of gold (0.24 nm) and thus suggests the formation of gold islands below the molecular layer. Such a morphology is in pronounced contrast to alkanethiols, where vacancy islands (also referred to as etch-pits) have been observed.^{54,55} In fact the formation of substrate islands was reported previously for other aromatic SAMs/Au(111) and seems to be characteristic for SAMs whose aromatic moiety is directly attached to the thiol^{56–59} or selenol^{60,61} headgroup.

The areas between these substrate islands exhibit an additional contrast variation in the form of darker patches separated by brighter areas. At higher magnification it becomes evident that these contrast variations correspond to a dense network of domains with a typical size of 5–15 nm as shown in Figure 6b. Within individual domains (e.g., dashed loop in Figure 6b) bright spots in characteristic zigzag lines can be identified which are oriented along $\langle 11\bar{2} \rangle$ azimuth directions and thus reflect the presence of rotational domains.

A typical high-resolution STM micrograph of a single rotational domain is presented in Figure 6c which provides detailed information on the molecular structure of the saturated AnT monolayer. Individual molecules can be resolved which are arranged in a quasi hexagonal fashion but with a rectangular superlattice (as indicated by the red unit cell). At first glance it may appear rather difficult to ascribe the molecular ordering of all parts of the STM image to a rectangular unit cell. A closer inspection, however, indicates that the data presented in Figure 6c reveal in fact three translation domains with two domain boundaries running across the image along the $\langle 11\bar{2} \rangle$ azimuth direction. For better visualization the same STM image is also displayed in Figure 6c after FFT filtering where the three different translational domains are marked by D1, D2, and D3 together with a rectangular unit cell for each domain. The dimensions of the unit cell for the monolayer phase have been derived from line scans taken for a single translational domain as shown in the bottom part of Figure 6c for area D1. Measurements which were taken from five different STM

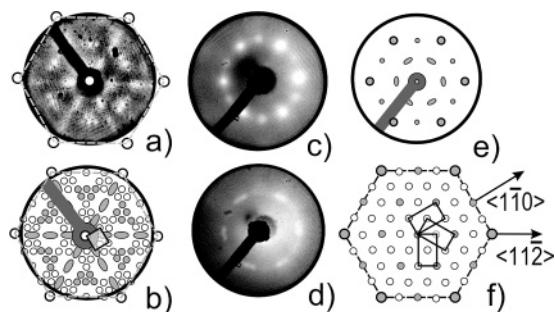


Figure 7. Summary of LEED data for AnT films on Au(111). The measured LEED pattern of a saturated monolayer ($E = 55$ eV) (a) is compared with the expected diffraction patterns (b) of a $(2\sqrt{3} \times 4)$ rect structure including rotational domains. The diffraction spots in the LEED patterns of the striped phase in panels c and d (157 eV and 40 eV, respectively) were combined schematically in panel e and are compared with panel f, the reciprocal lattice of a (4×2) phase including its rotational domains. The dashed hexagon and the larger circles represent the first-order diffraction spots of a clean Au(111) substrate, while the gray circles indicate the observed diffraction spots.

images yielded values of $a = 1.27 \pm 0.06$ nm for the $\langle 1\bar{1}0 \rangle$ direction and $b = 1.03 \pm 0.05$ nm for the $\langle 11\bar{2} \rangle$ azimuth. A comparison of the dimensions and orientation of such a rectangular unit cell with the underlying substrate lattice suggests the presence of a $(2\sqrt{3} \times 4)$ rect monolayer structure which is the closest structure commensurate with a Au(111) substrate and yields a theoretical unit cell size of $a_{\text{AnT}} = 1.15$ nm and $b_{\text{AnT}} = 1.00$ nm, respectively.

In Figure 6d a magnified high resolution STM image is shown which allows clearly the identification of four molecules within the rectangular unit cell. As shown by the line scan D in Figure 6c the molecules within the unit cell reveal a distinctly smaller corrugation height thus indicating the presence of different adsorption sites or local environments as compared to the molecules at the corners of the unit cell. To visualize a possible molecular ordering a simple model of AnT molecules forming a $(2\sqrt{3} \times 4)$ rect structure is shown for comparison in Figure 6d. In this model a face-on-edge herringbone arrangement of the aromatic backbone is assumed because this is a typical packing motif occurring in the crystalline structure of all acenes including anthracene.⁵² Though this gives a rather good agreement and reproduces the position of the four molecules within the unit cell seen by STM, a detailed structure model based on all experimental data will be discussed later.

Attempts to also image the diluted *striped phase* under ambient conditions failed and revealed only a rather rough and disordered surface. In view of the significant oxidation observed in the corresponding XPS data this is not surprising.

LEED. Although rather detailed information for the AnT-monolayer structure have been derived from STM data, additional electron diffraction experiments were carried to verify the commensurability of the adlayer and to obtain further information on the structure of the diluted striped phase.

Figure 7a displays a typical LEED pattern of the saturated AnT monolayer prepared from ethanolic solution. To suppress the inelastic background signal and to minimize the Debye–Waller attenuation of the diffraction peaks, all LEED data were recorded at a sample temperature of 120 K. Although only rather broad diffraction peaks with a weak contrast were observed, a distinct LEED pattern with additional diffraction spots is clearly recognized. Previous LEED experiments for alkanethiol-based

SAMs of various chain lengths have shown that the low contrast of the electron diffraction pattern is due to the small electron scattering cross section of C and S and a further attenuation in case of upright oriented backbones.⁶³ An important detail is the presence of adlayer-related diffraction spots for a large range of incident electron energies which suggests a commensurate structure. In contrast for a quasi-commensurate or incommensurate structure a Moiré type diffraction pattern is expected which reveals intense diffraction spots only at specific phase conditions.⁶⁴ A comparison with a simulated diffraction pattern for the $(2\sqrt{3} \times 4)$ rect superstructure presented in Figure 7b reveals a close correspondence of characteristic spot patterns (indicated by the filled circles). The broad diffraction peaks indicate the presence of a rather small average domain size which is in line with the STM data. Moreover, the streaky spots which appear along $\langle 11\bar{2} \rangle$ directions indicate the presence of lateral stacking faults of the molecular adlayer which can be attributed to translational domains. Attempts to also observe LEED patterns for an AnT monolayer prepared from acetone or DCM solution failed and only revealed rather diffuse substrate-related diffraction spots.

Further, it was possible to obtain diffraction patterns for the diluted monolayer after heating to 500 K (striped phase). In Figure 7c,d two typical LEED patterns are shown which were recorded at electron beam energies of 157 and 40 eV, respectively. Because we were unable to obtain diffraction patterns revealing simultaneously spots of different diffraction orders, the positions of the recorded spots have been combined according to the energy dependence of the Ewald sphere into a schematic diffraction pattern shown in Figure 7e. Considering again the presence of rotational domains leading to enhanced spot intensities when diffraction from all domains are superimposed (indicated by the filled circles in Figure 7f), the diluted phase can be identified as a (2×4) superstructure. The corresponding molecular structure model will be discussed below.

III. Discussion

In the present multitechnique study we have characterized the formation of anthracene-2-thiol SAMs on Au(111) as well as their microstructure and stability. It is shown that well ordered monolayer films can be prepared by immersion in ethanolic solution. However, because of the rather small solubility of acenes and their derivatives, intense rinsing is required to avoid a deposition of multilayer films. Moreover, a significant influence of solvents on the quality of the resulting films has been observed. Especially, for immersion in solutions from toluene, THF, or DMF, a pronounced decomposition of AnT molecules was found as evidenced by the corresponding RAIRS data which hampers the preparation of ordered AnT-SAMs. These effects were not observed for aliphatic or oligophenylene-based thiol-SAMs which have been studied previously in detail^{20–23} and thus emphasize the importance of a careful preparation of aromatic SAMs.

Our present observation is at distinct variance with previous experiments by Frey et al. where the preparation of ordered AnT-SAMs from DMF solution has been concluded based on

(63) Vollmer, S.; Witte, G.; Wöll, Ch. *Langmuir* **2001**, *17*, 7560.

(64) Kühnle, A.; Vollmer, S.; Linderoth, T. R.; Witte, G.; Wöll, Ch.; Besenbacher, F. *Langmuir* **2002**, *18*, 5558.

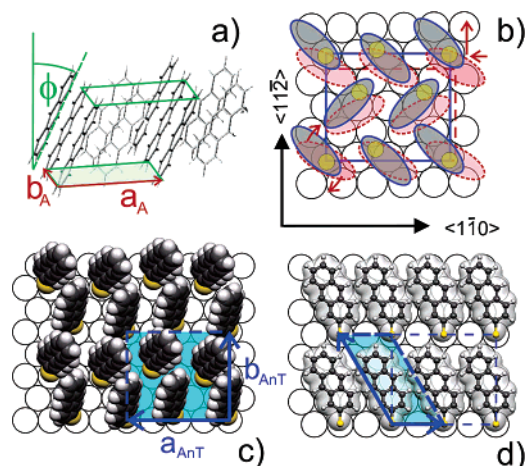


Figure 8. Molecular arrangement (a) of anthracene in the (001) plane of its crystalline phase and structure models of (c) the saturated monolayer of anthracene-2-thiol on Au(111) and (d) the diluted phase after heating above 450 K. Panel b shows the comparison of the anthracene bulk structure (red) with the $(2\sqrt{3} \times 4)_{\text{rect}}$ structure of the AnT-SAM (blue).

XPS and NEXAFS measurements.³⁵ Using TDS we have demonstrated that a DMF solution-based preparation yields only films of reduced coverage when compared to a saturated AnT monolayer prepared from ethanolic solution and thorough rinsing. Moreover, distinct differences in the fine structure and dichroism of the π^* -resonances were obtained for both preparations which further indicate a less dense packing for films from DMF preparation (see below). Since we have focused special diligence on using very clean solvents, as checked by NMR, contaminations can safely be excluded being the reason for such dilute films obtained by DMF preparation.

From our STM and LEED data a $(2\sqrt{3} \times 4)_{\text{rect}}$ structure has been identified for the saturated AnT monolayer. As regards the formation of such SAMs, it is instructive to first consider the corresponding crystal structure of the AnT backbone. Anthracene crystallizes in a monoclinic lattice with a layered structure.⁵² Within the layers, which correspond to (001) planes, the individual molecules adopt face-on-edge herringbone arrangement and form a rectangular unit cell given by $\mathbf{a}_A = 8.53$ Å and $\mathbf{b}_A = 6.01$ Å. The molecules reveal an upright orientation of their long axis forming an angle of $\phi = 34.8^\circ$ with respect to the plane normal as shown in Figure 8a. In van der Waals bond organic solids, such as alkanes, phenylenes, or acenes, this molecular tilt angle can be related to the packing density. In fact, it has been shown for alkanethiols^{65–67} that also in SAMs the resulting tilt angle of the backbone is directly related to the lateral packing density within the monolayer. From the unit cell of the saturated AnT monolayer a lateral molecular area of 28.7 Å² was derived which is somewhat larger than the corresponding value of anthracene in a (001) plane of 25.6 Å². Therefore a larger molecular tilting would be expected for the AnT-SAM as compared to the anthracene crystal which is in good agreement with a measured angle of $\phi = 43^\circ$. On the other hand a significantly larger tilt angle of $\phi = 52^\circ$ was determined for films prepared from DMF solutions which corroborates a reduced packing density.⁶⁸

Previous studies have shown that many organothiol-based SAMs form commensurate structures on Au(111) which can be related to preferential adsorption sites of the sulfur headgroups.^{1–3} Since the unit cell of the anthracene (001) plane does not directly fit the lattice of the gold substrate, an extended super cell has to be considered to provide repetitive adsorption sites. A comparison of the dimensions of the lateral unit cells of crystalline anthracene and the AnT-SAM reveals a rather large mismatch along the $\langle 11\bar{2} \rangle$ directions ($\mathbf{a}_A < \mathbf{b}_{\text{AnT}}$) which implies a significant expansion of 14% compared to the anthracene bulk structure. Along the $\langle 110 \rangle$ directions a close match between the $(2\sqrt{3} \times 4)_{\text{rect}}$ monolayer structure and the anthracene lattice is achieved by doubling of the anthracene unit cell which yields $2 \cdot \mathbf{b}_A \approx \mathbf{a}_{\text{AnT}}$. The small misfit (4%), however, causes a compression of the high-density structure favored in the bulk crystal and, thus, can lead to compressive stress. This stress within the layer can be relieved by formation of domain boundaries. Whereas the density of rotational domain boundaries for the AnT-SAM is comparable to SAMs of other aromatic systems prepared at similar conditions on Au(111),^{23,56,57,69} the very dense network of translational domain boundaries observed for this system has not been reported for any other aromatic system. Interestingly, these translational domains run always along the $\langle 11\bar{2} \rangle$ direction, i.e., alongside \mathbf{a}_{AnT} of the $(2\sqrt{3} \times 4)_{\text{rect}}$ structure. Therefore we suggest that their formation is most probably related to a reduction of the compressive stress along the $\langle 110 \rangle$ direction by formation of the observed dislocations. Our STM data revealed the presence of two types of translational domains for the AnT/Au(111) system. The first case can be exemplified by comparing domains D1 and D3 in Figure 6c, where a shift of about $\frac{1}{2} \cdot \mathbf{a}_{\text{AnT}}$ was observed. According to our model of the AnT structure this shift corresponds to the change in the phase of the azimuthal orientation of the aromatic backbones in the herringbone structure. The second case can be exemplified by comparing the domains D1 and D2 or D2 and D3 where a shift of about $\frac{1}{4} \cdot \mathbf{a}_{\text{AnT}}$ was observed. Most probably this corresponds to the change in the adsorption sites of molecules, e.g., from *hcp* to *fcc* on Au(111).

Interestingly similar translational domains have not been observed for biphenyl-based SAMs, although the misfit with the corresponding packing in the biphenyl crystal is even larger. In our opinion this difference is related to the fact that anthracene molecules are more rigid aromatic systems as compared to biphenyl, and therefore, changes in conformation of the molecule (e.g., twisting or bending), as another possibility to relieve stress instead of extensive domain boundary formation, are very limited. This conclusion is further corroborated by an improved long range ordering of aromatic SAMs when adding a flexible aliphatic spacer between the biphenyl backbone and the sulfur headgroup.⁷⁰

When comparing the molecular arrangement of anthracene-2-thiol SAMs with that of oligophenylene-based thiols, a further difference regarding the molecular symmetry has to be consid-

(65) Balzer, F.; Gerlach, R.; Polanski, G.; Rubahn, H. G. *Chem. Phys. Lett.* **1997**, 274, 145.

(66) Poirier, G. E.; Fitts, W. P.; White, J. M. *Langmuir* **2001**, 17, 1176.

(67) Barrena, E.; Ocal, C.; Salmeron, M. *J. Chem. Phys.* **2001**, 114, 4210.

(68) In their study Frey et al.³⁵ reported a surprisingly low average tilt angle of $\phi = 23^\circ$. At present we do not know the reason for the discrepancy, but we note that no details on film preparation (especially the rinsing) were given.

(69) Yang, G. H.; Qian, Y. L.; Engtrakul, C.; Sita, L. R.; Liu, G. Y. *J. Phys. Chem. B* **2000**, 104, 9059.

(70) Cyganik, P.; Buck, M.; Wilton-Ely, J. D.; Wöll, Ch. *J. Phys. Chem. B* **2005**, 109, 10902.

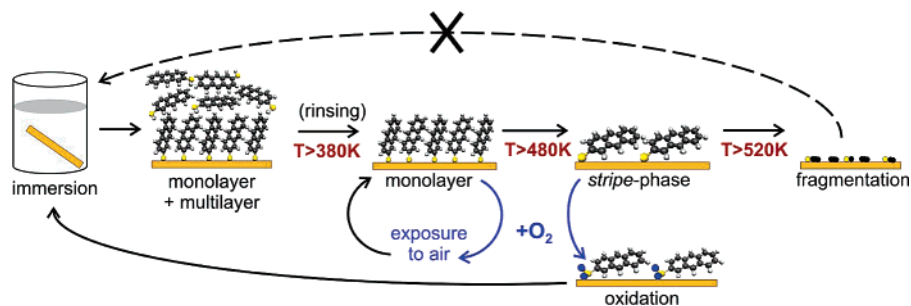


Figure 9. Schematic phase diagram showing the various phases of anthracene-2-thiol on Au(111) as a function of coverage and temperature.

ered. While thiols with a *p*-phenylene backbone are symmetric with respect to the long molecular axis, this symmetry is repealed in the case of AnT due to the sulfur addition. As a consequence AnT molecules are additionally canted upon chemisorption through the sulfur. In fact a closer inspection of high resolution STM images reveals a contrast variation for the different molecules within the unit cell, which suggests different adsorption sites and/or locally different surroundings. Considering the above-mentioned asymmetry of the canting we propose an alternating molecular arrangement for the AnT-SAM as shown in Figure 8b,c which is consistent with all experimental observations.

As regards the thermal stability of AnT-SAMs a partial desorption of about every second molecule occurs around 450 K. At the reduced coverage the remaining molecules have sufficient space to adopt a nearly flat adsorption geometry and form a (2×4) phase (Figure 8d). In this diluted *striped phase*, adsorption is stabilized by an additional interaction of the aromatic backbone with the metal substrate as evidenced by a significant broadening of the π^* -resonances in the NEXAFS spectra compared to that of the saturated monolayer. A quantitative analysis of the dichroism of these resonances yields an orientation of the transition dipole moment relative to the sample normal of $\alpha = 68^\circ$. The deviation from a perfectly normal orientation of the transition dipole moment can be related to a slight tilt of the aromatic backbone and/or to electronic distortions of the aromatic system upon chemisorption. Further heating causes a thermal cracking of molecules at temperatures above 520 K leading to a preferential desorption of sulfur-free fragments. Moreover, corresponding NEXAFS measurements indicate that the remaining carbon-containing fragments reveal no aromaticity and cannot be desorbed thermally but require a more rigorous cleaning by sputtering. Interestingly, in the case of even larger acenes such as pentacene, an intact desorption from Au(111) was observed which suggests the presence of significant stress within the aromatic backbone of AnT in the striped phase which favors their thermal fragmentation at elevated temperatures.

IV. Conclusions

The presently studied formation of AnT-SAMs on gold substrates can be summarized by a schematic phase diagram shown in Figure 9. Initially, upon immersion in (ethanolic) solution, films are formed which consist of thin multilayers on top of a chemisorbed thiolate monolayer. By intense rinsing (or gentle heating at 400–430 K under vacuum conditions) the excess of van der Waals bound material is removed and a saturated self-assembled monolayer is formed. This film, which consists of close-packed molecules adopting a $(2\sqrt{3} \times 4)$ *rect* unit cell, is rather stable and inert under ambient conditions. When heating the SAM above 450 K about half of the molecules desorb, while the remaining molecules form a dilute (4×2) phase with a nearly flat adsorption geometry. In contrast to the saturated monolayer this phase is chemically not inert and reveals a rapid oxidation of the sulfur headgroups under ambient conditions. Further heating above 520 K causes a fragmentation and cracking of the aromatic backbones of AnT. Interestingly, a saturated AnT-monolayer is again formed upon reimmersion of a partially oxidized (4×2) -phase, indicating a replacement reaction, while this is not possible for films which had been heated above 520 K.

Acknowledgment. This work has been funded by the Deutsche Forschungsgemeinschaft (DFG, focus program OFET). The authors are grateful to Dr. G. Beernink for assistance with some of the TDS experiments. D.K. acknowledges financial support from the Studienstiftung des Deutschen Volkes. P.C. is a postdoctoral fellow of the Alexander von Humboldt Foundation.

Supporting Information Available: Experimental details, sample preparation, and complete ref 9. This material is available free of charge via the Internet at <http://pubs.acs.org>.

JA0571592

Complete Ref. 9

Adams, D. M.; Brus, L.; Chidsey, C. E. D.; Creager, S.; Creutz, C.; Kagan, C. R.; Kamat, P. V.; Lieberman, M.; Lindsay, S.; Marcus, R. A.; Metzger, R. M.; Michel-Beyerle, M. E.; Miller, J. R.; Newton, M. D.; Rolison, D. R.; Sankey, O.; Schanze, K. S.; Yardley, J.; Zhu, X. Y. *J. Phys. Chem. B* **2003**, *107*, 6668.

Experimental Section

In the present study thin films of anthracene-2-thiol (AnT) prepared by immersion of gold substrates have been characterized by RAIRS, TDS, XPS, NEXAFS, STM, and LEED.

According to the sample requirements of the different techniques (e.g. size, planarity, coherence length) different types of gold substrates have been used throughout this study. Freshly evaporated gold/mica substrates were used for the STM measurements while the RAIRS, XPS and NEXAFS data were acquired for gold films deposited on Si-wafer. Au single crystals exposing a (111)-surface were used for the LEED and TDS measurements. The gold films were prepared in a deposition chamber operated at a base pressure of $\sim 10^{-7}$ mbar by evaporating (150nm) gold (99.995%, Chempur) onto Si-wafer or mica substrates at room temperature or at 580K, respectively. Before deposition the freshly cleaved mica sheets had been heated at 580K for about 24h under vacuum conditions to remove residual crystal water while the (100) oriented and polished silicon wafer were first covered with a 5nm titanium adhesion layer. Thickness and deposition rate (20Å/s) were monitored using a crystal oscillator (Leybold Inficon). After deposition, the gold/mica substrates were flame-annealed in abutane/oxygen flame prior to the adsorption experiments. This procedure yielded high-quality Au-films with flat terraces of several 100nm exhibiting a (111) surface orientation. The Au(111) single crystals were cleaned in UHV by repeated cycles of Ar⁺-sputtering (700eV) and annealing before immersion.

Anthracene-2-thiol was synthesized as described previously¹⁾ and all AnT-films were prepared by immersion of the gold substrates in 0.1-0.3mM solutions at room temperature. Various solvents (purity >99%) including toluene, tetrahydrofuran [THF], dimethylformamide [DMF], dichloromethane [DCM], acetone and ethanol have been used. After removal from the solution, the substrates were thoroughly rinsed with the corresponding pure solvent and dried in a nitrogen stream.

The XPS, TDS and LEED measurements were carried out in a multi-technique UHV instrument which has been described in detail elsewhere²⁾. LEED patterns were recorded by using a microchannel plate LEED system (OCI) which allows operation at incident beam currents as low as 0.05-0.1 nA/mm² to minimize electron beam damages of the organic adlayers. A quadrupole mass spectrometer (Balzers QMS200, mass range 0-300amu) with a Feulner cup was used to record thermal desorption spectra (TDS) by employing a computer controlled linear heating ramp³⁾. The apparatus is further equipped with a X-ray photoelectron spectrometer consisting of a twin-anode (VG) and a hemispheric energy analyzer (Leybold EA200).

All RAIRS measurements were carried out using a dry-air purged BioRad Excalibur FTS-3000 FTIR-spectrometer. Monolayer spectra were recorded in grazing incidence reflection mode at a fixed angle of 84° relative to the surface normal using *p*-polarized light. The reflected light was detected by a liquid nitrogen cooled MCT narrow band detector. All SAM spectra were acquired with a resolution of 1cm^{-1} . For background compensation all data were normalized by subtraction of a spectrum which was recorded for a perdeuterated docosanethiol-SAM on gold. This provides a reference sample which is protected against unintentional contaminations by adsorption from the environment as compared to a clean gold surface. The IR spectra from bulk samples (KBr-pellet) were recorded using a DTGS detector.

The NEXAFS measurements were performed at the synchrotron storage ring BESSY II in Berlin (Germany) at the dipole beam line HE-SGM using an end-station described in details elsewhere⁴⁾. All NEXAFS measurements were carried out with linear polarized synchrotron light with a polarization factor of $\sim 85\%$ and an energy resolution of about 300meV at the C K-edge. The NEXAFS spectra were recorded in a partial electron yield mode using a homemade electron detector based on a channel plate and a retarding field of -150V. The energy calibration of all NEXAFS spectra is carried out by recording simultaneously with each spectrum the photocurrent of a carbon contaminated gold grid. This signal reveals a characteristic peak at a photon energy of 284.9eV⁵⁾ which had been calibrated by a graphite sample before. Moreover, the photocurrent on the grid is used as a radiation flux monitor. The NEXAFS raw data have been normalized in a multi step procedure by considering the incident photon flux and the background signal of the clean substrate (for details see Ref. (4)).

STM measurements were carried out in air, using a Jeol JSPM 4210 microscope. The tips were prepared mechanically by cutting a 0.25mm Pt_{0.8}Ir_{0.2} wire (Goodfellow). All data were collected in a constant-current mode with a tunneling current of 200pA and a sample bias of -200mV (tip positive). For these tunnelling conditions no tip-induced changes were observed.

(1) Heffter, W. *Ber. dtsch. chem. Ges.* **1895** 28, 2258.

(2) Loepp, G; Vollmer, S.; Witte, G.; Wöll, Ch. *Langmuir* **1999**, 15, 3767.

(3) Lukas, S.; Vollmer, S.; Witte, G.; Wöll, Ch. *J. Chem. Phys.* **2001**, 114, 10123.

(4) Reiss, S.; Krumm, H.; Niklewski, A.; Staemmler, V.; Wöll, Ch. *J. Chem. Phys.* **2002**, 116, 7704.

(5) NIST X-ray Photoelectron Spectroscopy Database 20, Version 3.4 (Web Version), <http://srdata.nist.gov/xps/>